Wind Wave Growth at Short Fetch

T. LAMONT-SMITH* AND T. WASEDA+

Department of Environmental and Ocean Engineering, University of Tokyo, Tokyo, Japan

(Manuscript received 10 October 2006, in final form 17 December 2007)

ABSTRACT

Wave wire data from the large wind wave tank of the Ocean Engineering Laboratory at the University of California, Santa Barbara, are analyzed, and comparisons are made with published data collected in four other wave tanks. The behavior of wind waves at various fetches (7–80 m) is very similar to the behavior observed in the other tanks. When the nondimensional frequency F^* or nondimensional significant wave height H^* is plotted against nondimensional fetch x^*, a large scatter in the data points is found. Multivariate regression to the dimensional parameters shows that significant wave height H_{sig} is a function of U^2x and frequency F is a function of $U^{1.25}x$, where U is the wind speed and x is the horizontal distance, with the result that in general for wind waves at a particular fetch in a wave tank, approximately speaking, the wave frequency is inversely proportional to the square root of the wind speed and the wavelength is proportional to the wind speed. Similarly, the wave height is proportional to $U^{1.5}$ and the orbital velocity is proportional to U. Comparison with field data indicates a transition from this fetch law to the conventional one [the Joint North Sea Wave Project (JONSWAP)] for longer fetch. Despite differences in the fetch relationship for the wave tank and the field data, the wave height and wave period satisfy Toba's 3/2 power law. This law imposes a strong constraint on the evolution of wind wave energy and frequency; consequently, the energy and momentum retention rate are not independent. Both retention rates grow with wind speed and fetch at the short fetches present in the wave tank. The observed retention rates are completely different from those typically observed in the field, but the same constraint (Toba's 3/2 law) holds true.

1. Introduction

Waves grow in the presence of wind as long as the wind speed is greater than the phase velocity of the waves. The wave height, and hence the energy of the waves and the wavelength, increases with the wind speed and the fetch. Empirical fetch laws have been sought to describe sea state as functions of the wind speed and fetch in nondimensional form. Wilson (1965) was one of the first to provide fetch formulas, and more recent examples include Kahma and Calkoen (1992) and Battjes et al. (1987), whose work is based on the influential Joint North Sea Wave Project (JONSWAP) results of Hasselmann et al. (1973). Komen et al. (1994) also discuss various fetch laws. Dimensional analysis leading to the derivation of these fetch laws is provided in the pioneering works of Tulin (1994) and Fontaine (2001). Donelan et al. (1992), however, have called into question the very idea of a universal fetch-limited growth law that can be applied under different circumstances, and Badulin et al. (2007) suggest instead that wave growth depends only on the locally determined rate of dissipation rather than on external attributes such as wind speed.

It is conventional when analyzing wave data to use nondimensional units; the wind speed and the acceleration due to gravity are used to nondimensionalize the various quantities such as frequency and wave height. When the wave wire data from the University of California at Santa Barbara (UCSB) wave tank were first examined using nondimensional quantities, there was a very wide scatter in the data points, which was not necessarily present when dimensional values were used. As a result, this paper will use dimensional data values to derive the relationships among the wind speed, the fetch, and the resulting dominant wave frequency and wave height. This means that at times inelegant fractional quantities will be plotted, but this has the benefit

* Current affiliation: QinetiQ (Ltd.), Malvern, United Kingdom.
+ Current affiliation: Department of Ocean Technology Policy and Environment, Graduate School of Frontier Sciences, University of Tokyo, Tokyo, Japan.

Corresponding author address: T. Lamont-Smith, QinetiQ, St Andrew's Road, Malvern, Worcs. WR14 3PS, United Kingdom.
E-mail: tlsmith@qinetiq.com

DOI: 10.1175/2007JPO3712.1

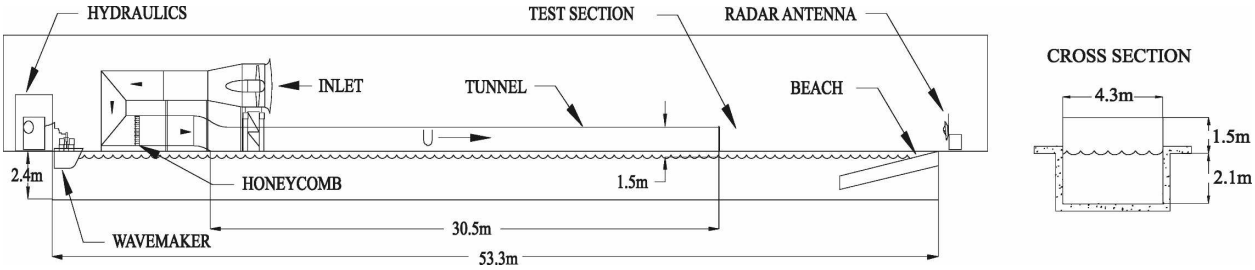

FIG. 1. Sketch of the wave tank at the University of California, Santa Barbara.

of reducing the data spread, leading to much less scatter in the graphs. The motivation of this study is to investigate the fetch laws for short fetch.

2. Wave tank experiment

Figure 1 shows a sketch diagram of the UCSB wave tank. Figure 2 shows the dominant frequency F of the wind waves measured using the Ocean Engineering Laboratory (OEL) C-band radar at a fetch of 35 m (discussed elsewhere; Lamont-Smith et al. 2003). Also shown on the same graph are results published by Rozenberg et al. (1999) collected using a single wave wire at a fetch of 11 m in the Scripps Institute of Oceanography (SIO) wave tank (shown as triangles) and at a fetch of 80 m in the Delft Hydraulics Laboratory large wave tank (crosses). The lines plotted in Fig. 2 are all of the form $F \propto U^{-0.5}$ and fit the data well, except at the very lowest wind speeds. The wind speed was measured at a height of 50 cm in each wave tank. The data points from the three wave tanks are offset from each other as a result of the tanks' different fetches. These results suggest that fetch laws could be found that may be generally applicable to wave tanks and short fetches.

The OEL C-band radar collects data sampled in range with a resolution of 0.0377 m. A 2D Fourier transform of data collected with a wind speed of $U = 3.4$ m s^{-1} produces the ω–k diagram shown in Fig. 3. Overlaid on the plot are lines describing the deep water gravity wave dispersion curve; that is,

$$\omega_n = \sqrt{nk_n g} + k_n v_{\text{drift}}. \quad (1)$$

The solid line shows the gravity wave dispersion line ($n = 1$) in still water. The dotted lines show the dispersion curves for the nth harmonics when the drift current v_{drift} is taken into account. The drift current as estimated from the data in this case is $v_{\text{drift}} = 0.06 \pm 0.01$ m s^{-1}. Other measurements at higher wind speeds (and larger waves) suggest that the drift current measured by the radar is approximately 1% of the wind speed. The wavelength L of the waves measured by the radar is not directly affected by the drift current and was found to scale linearly with the wind speed (i.e., $L \propto U$). Lamont-Smith et al. (2003) used the radar data to investigate the presence of wave groups and spectral downshifting with fetch in the wave tank, and they observed that the waves change frequency in discrete steps associated with wave breaking events. Fuchs and Tulin (2000) found that the radar data could also give an estimate of the surface height spectrum, which was comparable to wave wire spectra; here, only the wave wire data will be analyzed in any detail.

a. Frequency dependence

An experiment was conducted in the UCSB wave tank in 1998 in which an array of 10 wires was positioned along the tank and data were collected at five different wind speeds. The variations in the peak frequency of the measured height spectra are shown in Fig. 4 as a function of distance down the tank. Data from the shortest fetch (4 m) are not shown because the measured frequency was significantly lower than ex-

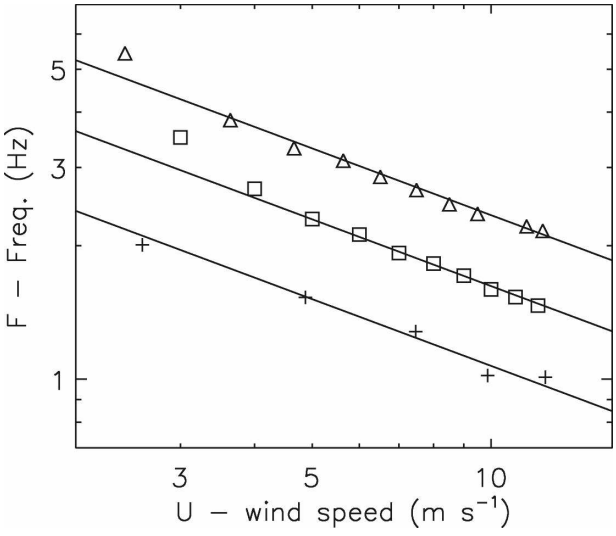

FIG. 2. Dominant wave frequency in different wave tank environments vs wind speed: 80-m fetch, Delft wave tank (crosses), 35-m fetch, UCSB wave tank (squares), and 11-m fetch, SIO wave tank (triangles).

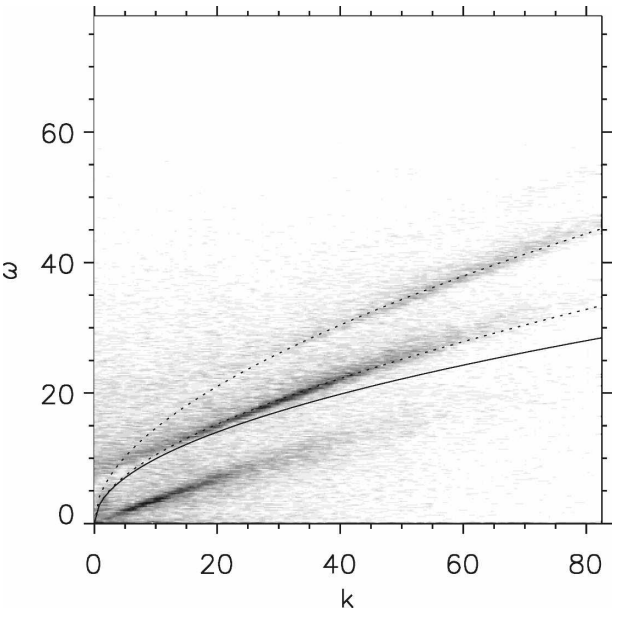

FIG. 3. Two-dimensional Fourier transform of radar range–time intensity radar data plot of ω–k. The solid line is the gravity wave dispersion relation; dotted lines show the dispersion line and its harmonic in the presence of a current.

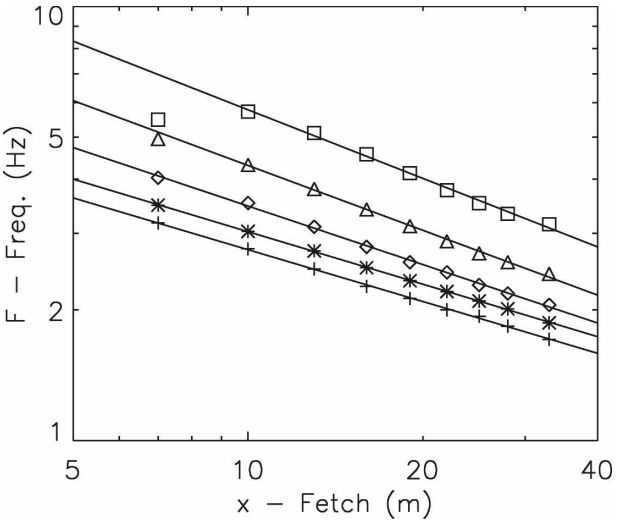

FIG. 4. Dominant wave frequencies in the UCSB wave tank environment vs fetch for different wind speeds: 10.3 (crosses), 9.7 (asterisks), 8.4 (triangles), 5.7 (diamonds), and 3.4 m s^{-1} (squares).

pected for all wind speeds, which was probably a problem associated with the estimation of the peak frequency for the very low spectral energies present. For the higher wind speeds, the fetch dependence is approximately $F \propto x^{-0.4}$, but this relationship does seem to be dependent on wind speed to a certain extent.

In general, a nondimensional fetch law for the frequency may be written as

$$\frac{Fu_*}{g} \propto \left(\frac{xg}{u_*^2}\right)^{-\alpha}. \tag{2}$$

The relationship found from the JONSWAP data (Hasselmann et al. 1973) is widely preferred in the literature, with $\alpha = 0.33$. Other empirical values of the exponent α from various observations are summarized in Table 1.

The wind speed U that is used here is the average velocity in the wind tunnel 50 cm above the still water surface. Nondimensional quantities such as F^*, H^*, and x^*, where $F^* = FU/g$, $H^* = Hg/U^2$, and $x^* = xg/U^2$, are often used in plotting this kind of wind wave data. Thus, Eq. (2) may be rewritten as

$$F^* = Cx^{*-a}, \tag{3}$$

where C is assumed to be a nondimensional constant.

Figure 5 shows a scatterplot of the nondimensional quantities F^* versus x^*. There is a wide spread in the values; although a dotted line of the form $F^* = 3x^{*-0.38}$ can be drawn through the large wind speed values, this relation leaves out cases with lower wind speeds.

One way to establish the relationship between the wind speed and the fetch is to use a contour plot on log-scale paper showing the isofrequencies, as in Fig. 6. The advantage of displaying the data in this way is that no assumption is made about the relationship between the wind speed and the fetch. The isofrequencies seem to be parallel to the dotted lines of the form $\log(U) = -0.8 \log(x) + \text{constant}$; hence, Fig. 7 replots the data against the quantity $U^{1.25}x$. For waves of frequency less than 4 Hz (or wavelengths larger than 10 cm) the data is well reproduced by a best-fit line of the form

$$F \propto (U^{1.25}x)^{-0.43}. \tag{4}$$

Performing a multivariate fit gave an exponent of 1.3 ± 0.05 for U, and the overall exponent (outside the bracket) was -0.43 ± 0.01. Thus, the frequency is approximately proportional to $U^{-0.5}$, and it is approximately proportional to $x^{-0.4}$. Equation (2) may be rearranged to show the frequency dependence on the fetch and the wind speed; that is,

TABLE 1. Fetch laws from various observations.

Dataset	α	β
Phillips (1977) equilibrium	0.25	0.5
Toba's 3/2 law	1/3	1/2
Donelan (1985)	0.27	0.48
Mitsuyasu et al. (1980)	0.33	0.54
JONSWAP	0.33	0.5
Hwang et al. (1996)	0.2368	0.4053
Burling (1959)	0.225	0.427
Kahma (1981)	0.27	0.45

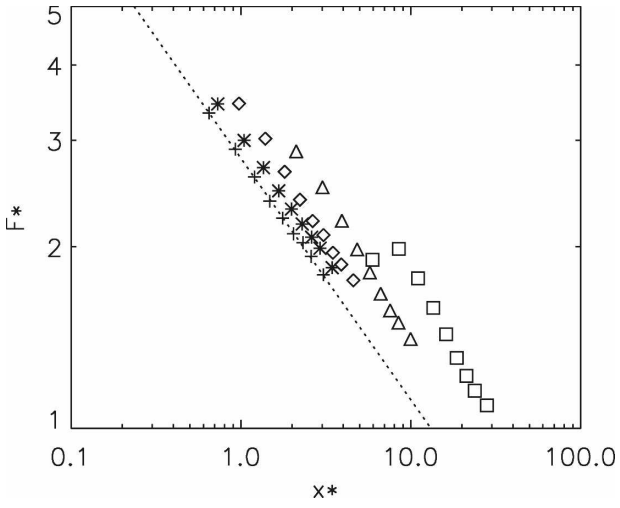

FIG. 5. A scatterplot of the nondimensional quantities F^* and x^*. Symbols as in Fig. 4.

$$F \propto x^{-\alpha}, \quad \text{and}$$
$$F \propto u_*^{2\alpha-1}. \tag{5}$$

A graph of the wind exponent (for U rather than u_*) versus the fetch exponent for the nondimensional frequency fetch law has a straight-line relationship [defined by (5) but not shown] that must be obeyed if the nondimensional relationship is valid. Field measurements listed in Table 1 give specific values of α. These wave tank results are some way from conforming to the nondimensional equation relationship expected in (5). The measured frequency dependence is closest to the JONSWAP result where $\alpha = 0.33$, but it differs from this nondimensional result by a factor $(U^2x)^{-0.1}$, which suggests that in the wave tank C is not a constant; rather,

$$C \propto (U^2x)^{-0.1}. \tag{6}$$

There are a number of possible explanations for this result. For instance, the drift current has an influence on the measured frequency, particularly at high frequencies; however, the effect of drift current is quantified in Fig. 3, and the influence is believed to be minimal. It is not clear whether using the wind friction velocity u_* would be better at reducing the scatter than using U. For instance, one can argue that the friction velocity should grow with fetch. The drag coefficient C_D for the friction velocity can depend on the wave age (Jones and Toba 2001). Unpublished reports from previous work indicate that the evolution of the friction velocity is not straightforward in the UCSB wave tank; however, the scatter of data is much larger than can be comfortably explained by differences in the drag coefficient.

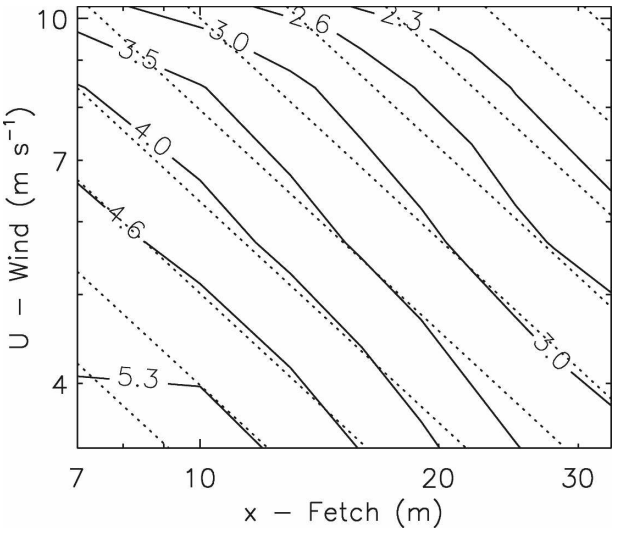

FIG. 6. A contour plot on log–log coordinates showing the lines of constant frequency (solid) calculated from the UCSB frequency data. The dotted lines are of the form $\log(U) = -0.8 \log(x) + \text{constant}$.

b. Wave height dependence

A scatterplot of the nondimensional quantities H^* and x^* in Fig. 8 shows a large scatter of the data points, allowing only tenuous relationships to be drawn. A dotted line of the form $H^* = 0.03x^{*0.32}$ is plotted in Fig. 8 and appears to show a limit for the large fetch values. The formula for the nondimensional fetch law for the wave height has a relationship of the form

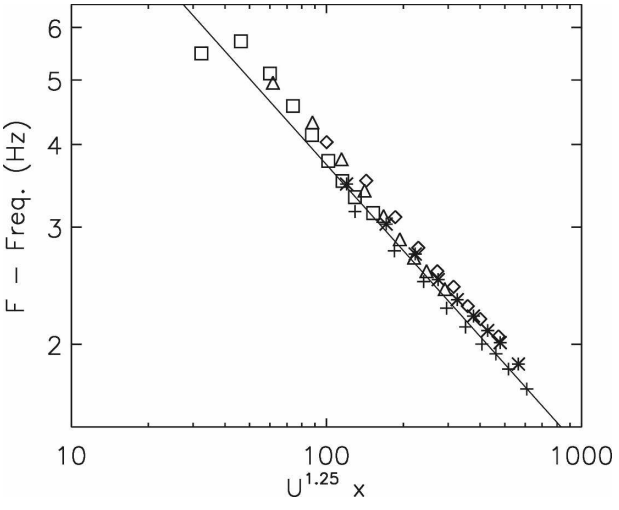

FIG. 7. A scatterplot of the peak frequency of the wind wave vs the quantity $U^{1.25}x$. The line is of the form $F \propto (U^{1.25}x)^{-0.43}$. Symbols as in Fig. 4.

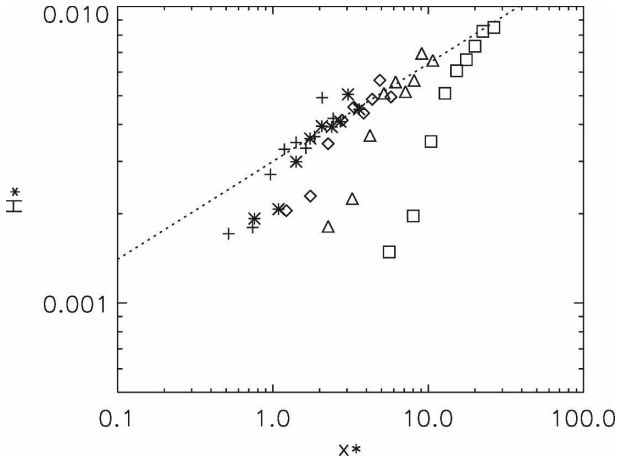

FIG. 8. A scatterplot of the nondimensional quantities H^* and x^* with a dotted line of the form $H^* = 0.03x^{*0.32}$, which appears to show a limit. Symbols as in Fig. 4.

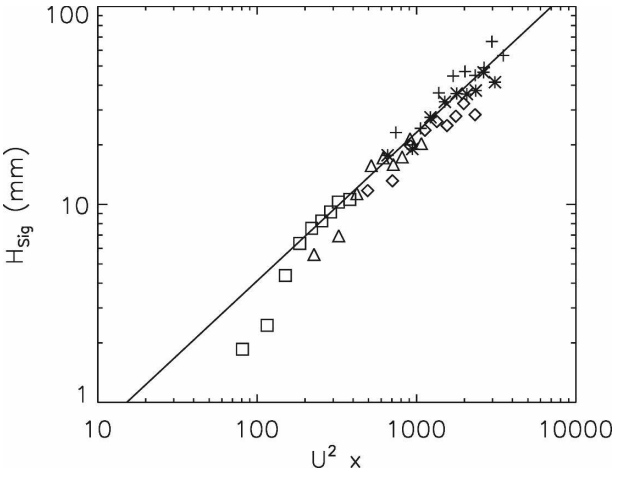

FIG. 9. A scatterplot of the significant wave height H_{sig} of the wind waves vs the quantity U^2x. The line is of the form $H_{sig} \propto (U^2x)^{0.75}$. Symbols as in Fig. 4.

$$H^* = Dx^{*\beta}. \tag{7}$$

Performing a multivariate fit analysis similar to that performed for the frequency data suggests that replotting the wave height data against the quantity U^2x, as in Fig. 9, substantially reduces the scatter in data points compared to Fig. 8. The straight line is of the form

$$H_{sig} \propto (U^2x)^{0.75}. \tag{8}$$

This demonstrates that the significant wave height is approximately proportional to $U^{1.5}$ and $x^{0.75}$. The multivariate analysis gives the exponent outside the bracket as 0.76 ± 0.03, and the exponent inside the brackets for U is 2.2 ± 0.2.

The wave height dependence is consequently stronger than expected from the conventional nondimensional Eq. (7), which may be rewritten as

$$H_{sig} \propto x^{\beta}, \quad \text{and}$$
$$H_{sig} \propto U^{2-2\beta}. \tag{9}$$

Once again, the measured results are closest to the JONSWAP result where $\beta = 0.5$, but the wave height dependence differs from this nondimensional result by a factor $(U^2x)^{0.25}$, which suggests that, like C, D is not a constant but rather is a function of U^2x:

$$D \propto (U^2x)^{0.25}. \tag{10}$$

c. Toba's law

Toba's 3/2 power law (Toba 1972) relates the nondimensional significant wave height to the frequency as shown:

$$H^* \propto F^{*-1.5}. \tag{11}$$

Equation (11) has been widely confirmed in the literature for both wave tank and open ocean data (Masuda and Kusaba 1987), and Fig. 10 shows that the UCSB data also conform to Toba's 3/2 power law in that $H^* \propto F^{*-1.5}$, at least for the larger waves in the tank. Waves with wave height less than 4 mm or wave frequency greater than 5 Hz are shown by crosses, and these points were discarded in fitting the line to the data.

If the JONSWAP values for α and β are assumed, then C and D may be evaluated from (3) and (7), and these quantities are shown in Fig. 11. The data in Fig. 11 are plotted against the nondimensional quantity $U^2x/g\zeta^2$, where a length $\zeta = 1$ has been introduced to make the abscissa quantity dimensionless. The diamonds show the quantity $C^{-1.5}$ calculated from the wave frequency, and the squares show D calculated from the significant wave height. It is worth noting that Toba's law implies that $H^*F^{*1.5}$ should be constant, and therefore that $\beta/\alpha = 3/2$, so that there is no x^* fetch dependence, and $H^*F^{*1.5} = C^{1.5}D = B$. As expected from the previous analysis, neither C nor D is constant. The solid lines are parallel with a gradient of 0.15 on the log–log paper, which is the relationship expected for $C^{-1.5}$ from (6), and the lines are separated by the quantity $B = 0.01$, which is close to the value estimated in Fig. 10 ($B = 0.012 \pm 0.02$). The solid line overlaid on the values of D does match the data points relatively well, where $D \propto (U^2x/g\zeta^2)^{0.15}$. The dashed line matches the data slightly better than the solid line (in fact, it shows the relationship for D from (10) based on the earlier analysis) and has a gradient of 0.25 on the log–log paper.

Combining (6) and (10) from the earlier analysis, it can be seen that some wind speed and fetch dependence should be expected to still be present; thus,

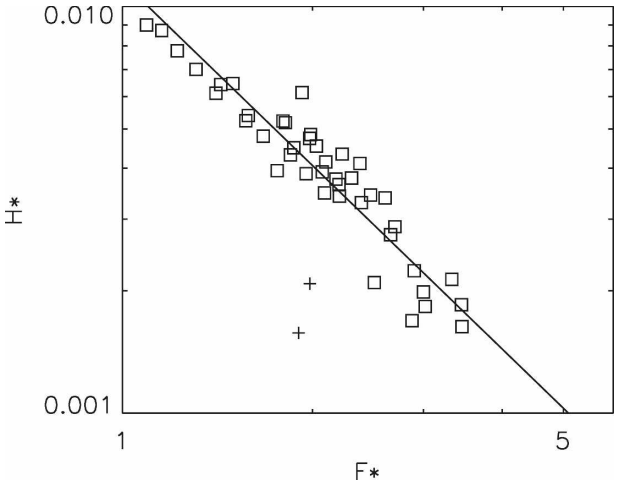

FIG. 10. A scatterplot of the nondimensional quantities H^* and F^*, with a solid line of the form $H^* = 0.012F^{*-1.5}$, which has the correct exponent for Toba's law. Squares indicate data points used for the line fit, with wave height greater than 4 mm and frequency less than 5 Hz; crosses indicate the smaller waves.

$$H^*F^{*-1.5} \propto (U^2x)^{0.1}. \tag{12}$$

Examination of the quantity $H^*F^{*1.5}$ indicates that it is approximately constant (not shown) with no clear trends with either U or x or indeed with U^2x, as suggested by (12). The weak dependence of $H^*F^{*1.5}$ on U, x, or U^2x suggests that Toba's relationship is a universal law for evolving wind sea, regardless of the distinct fetch laws satisfied in the field and in the wave tank (which indicates that the solid lines in Fig. 13 are in fact the preferable representation of the data). The 3/2 power law (11) derives from the evolution of wave energy and momentum, as suggested by Toba (1972). Thus, what the law imposes is a constraint that relates the evolution of the energy and momentum of the wind sea. Tulin (1994) and Fontaine (2001) have analytically derived the conventional fetch laws, taking into account Toba's law. An unexpected finding of this study is that the wind waves in the tank follow fetch laws quite distinct from those in the field, and yet Toba's law is still satisfied. The wind sea regime in the wave tank therefore appears to be a transition regime from a wind sea with an extremely short fetch (e.g., Waseda et al. 2001) to a growing wind sea in the open ocean (e.g., JONSWAP).

3. Other wave tank experiments

A number of other researchers have presented wave tank data of wind waves, including Toba (1972), Donelan et al. (1985), and Rozenberg et al. (1999). The average wind speed measured in each of the tanks was measured at a height of 50 cm, except for Donelan's

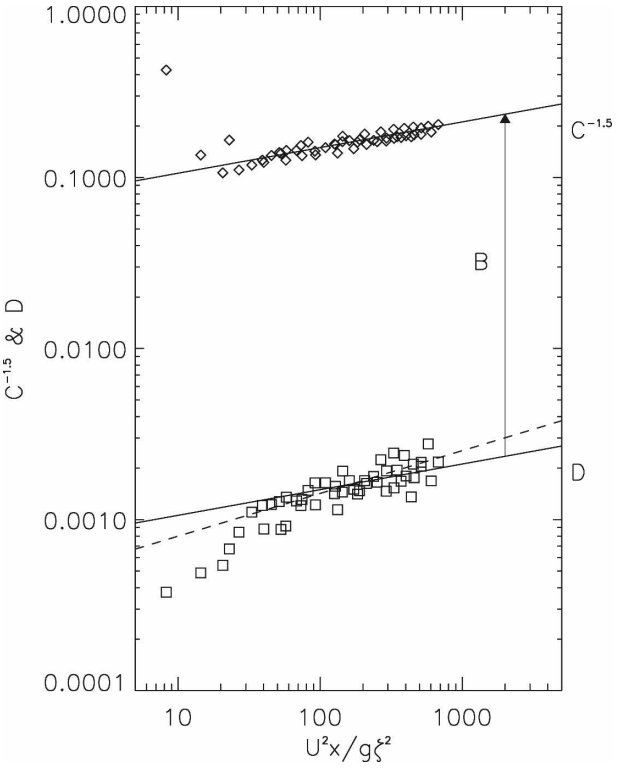

FIG. 11. Values of $C^{-1.5}$ and D evaluated from the UCSB data of frequency (diamonds) and significant wave height (squares). The solid lines have a gradient of 0.15 and are separated by a factor of $B = 0.01$; the dashed line has a gradient of 0.25.

data, which was measured at a height of 26 cm. The equivalent speed at a height of 10 m was also given. A logarithmic wind profile under neutral stability conditions has been assumed here to convert the wind speed data to a height of 50 cm. This produced a small percentage change (approximately 10%) in the wind speed values compared to the 26-cm height.

The dimensional data for the wave tanks mentioned are plotted in Figs. 12 and 13 with frequency F versus $U^{1.25}x$ and average wave height H_{av} versus U^2x, respectively. In Fig. 12, the line is of the same form as found for the UCSB data in (4), with $F \propto (U^{1.25}x)^{-0.43}$. A multivariate analysis of this data gives a best fit with the wind exponent of 1.4 ± 0.1 and the overall exponent outside the brackets of -0.40 ± 0.01, compared to the exponents of 1.30 ± 0.05 for U and -0.43 ± 0.01 found previously for the UCSB wave frequency data. The data from Donelan et al. (1985) shown by the square symbols does not fit the line in Fig. 12 closely, which accounts for the small difference in the exponent of -0.40 (rather than -0.43 that was calculated previously).

Similarly in Fig. 13, the solid line is of the form $H_{av} \propto (U^2x)^{0.75}$, just as for the UCSB results in (8). The mul-

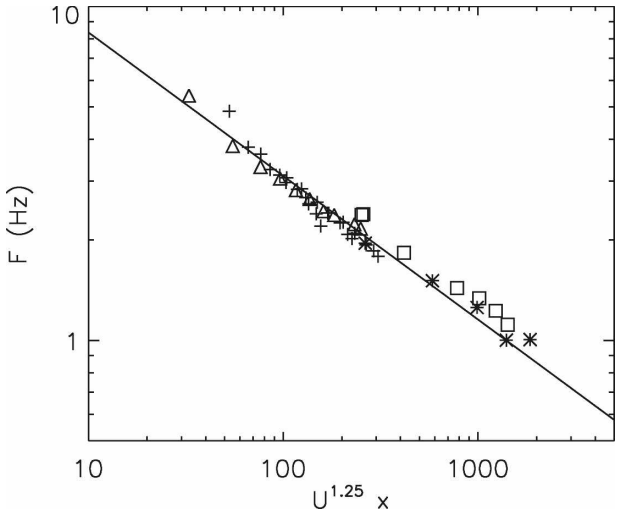

FIG. 12. A scatterplot of the peak frequency of the wind waves vs the quantity $U^{1.25}x$: Toba (cross), SIO (triangle), Delft (asterisk), and Donelan (square). The line is of the form $F \propto (U^{1.25}x)^{-0.43}$.

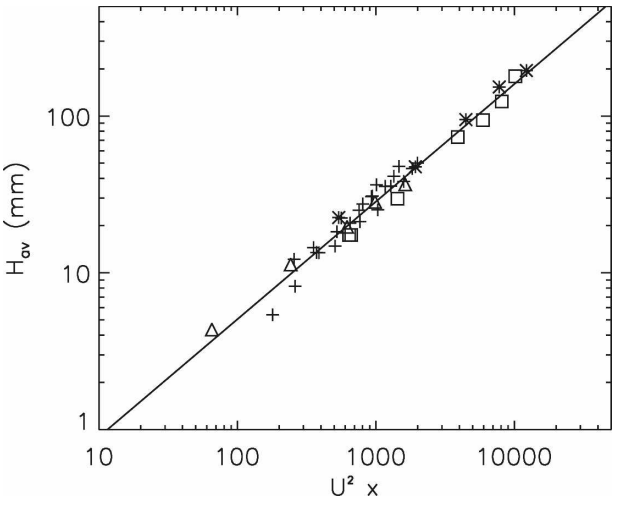

FIG. 13. A scatterplot of the average wave height of the wind waves vs the quantity U^2x. The line is of the form $H_{av} \propto (U^2x)^{0.75}$. Symbols as in Fig. 12.

tivariate analysis of this data gives a best fit with the wind exponent of 2.1 ± 0.1 and the overall exponent outside the brackets of 0.74 ± 0.02, compared to the exponents 2.2 ± 0.1 for U and 0.76 ± 0.03 found previously for the UCSB wave height data. The agreement of the multivariate analysis for the UCSB data and the other wave tanks is very close and is within the error bars of the analysis. The conventional nondimensional quantities (H^* and F^*) for Toba's data have been plotted elsewhere by Tokuda and Toba (1982), who observed a large scatter in the nondimensional quantities, particularly H^*, exactly as observed for the UCSB data in Fig. 8.

4. Comparison with field data

Most field measurements show nondimensional frequency or height plotted versus the nondimensional fetch. The fetch measurements can span many decades, but measured wind speed in the field typically varies by significantly less than even one decade. It is also very hard to find steady wind conditions, particularly over large distances. As a result, the wind speed dependence identified from the wave tank data cannot easily be confirmed (or denied) using field data. An interesting experiment would be to collect wave data in a narrow body of water like a loch or fjord, where the wind speed can vary in strength with time but tends to blow consistently either up or down the loch, thereby giving consistent fetches. This would allow the wind speed dependence to be investigated out to larger fetches than is possible in wave tanks.

Figures 14 and 15 show UCSB data, along with wave data collected by Walsh et al. (1989) and by Burling (1959) from the open ocean and a reservoir, respectively. These datasets are unusual in that the data are presented with dimensional units rather than in a nondimensional form and so can be analyzed here. The UCSB wind speed values have been extrapolated to produce U_{10}, the wind speed at 10 m above the water surface, so the data may be compared with the field measurements. The waves in the paper by Walsh et al. (1989) become fully developed at a certain fetch (~200 km), and no data beyond that fetch are shown here.

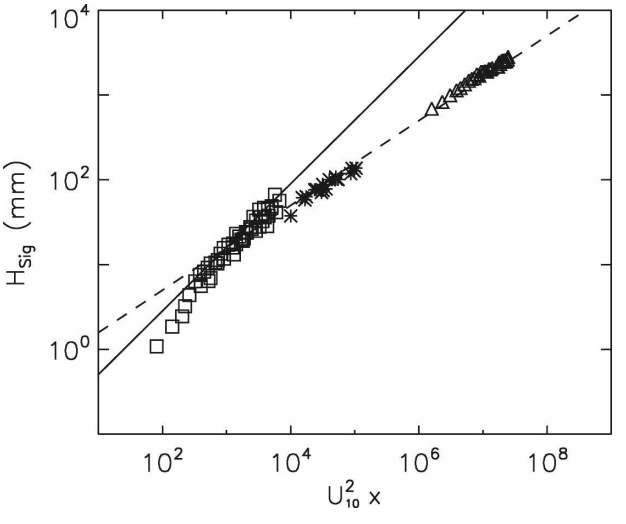

FIG. 14. A scatterplot of significant wave height of the wind waves vs $U_{10}{}^2x$, with data from Walsh (triangles), Burling (asterisks), and UCSB (squares). Solid line: $H_{sig} \propto (U_{10}{}^2x)^{0.75}$; dashed line: $H_{sig} \propto (U_{10}{}^2x)^{0.5}$.

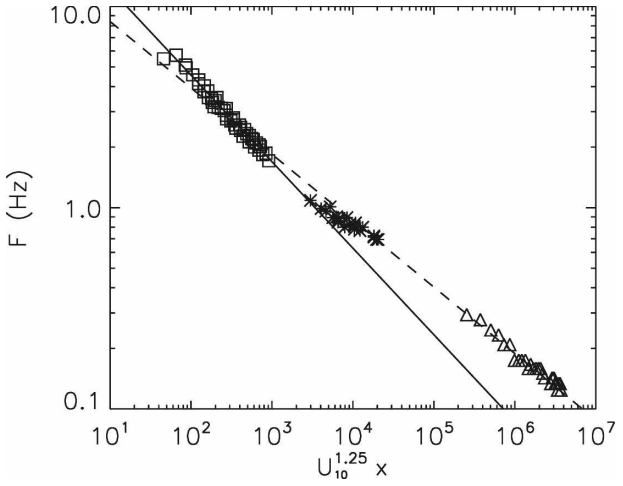

FIG. 15. A scatterplot of the frequency of the wind waves vs $U_{10}{}^{1.25}x$. Solid line: $H_{sig} \propto (U_{10}{}^{1.25}x)^{-0.43}$; dashed line: $H_{sig} \propto (U_{10}{}^{1.25}x)^{-0.33}$. Symbols as in Fig. 14.

Figure 14 shows a scatterplot of H_{sig} versus the quantity $U_{10}{}^2x$ for the different datasets and with a dashed line showing the JONSWAP relationship of the form $H^* = Dx^{*0.5}$, where D ($=0.0017 \pm 0.0002$) is a constant. The data from Walsh et al. (1989) are indicated by triangles and those from Burling (1959) and the UCSB data are asterisks and squares, respectively; the solid line shows the relationship (8) found in Fig. 10 for the UCSB wave tank data. The wave tank data clearly exhibit different growth behavior from that shown by the field data.

It is less easy to display the frequency data from the field and tank together. Figure 15 shows a scatterplot of the quantity $U_{10}{}^{1.25}x$ versus the peak frequency of the wind waves. The dashed line is of the form $F \propto (U_{10}{}^{1.25}x)^{-0.33}$, which is similar to the JONSWAP result for the fetch exponent, but the exponent for the wind is different. Frequency F versus $(U_{10}x)^{-0.33}$ would be a straight line for the JONSWAP relationship. The Walsh data were all collected at a single wind speed, and the Burling data have a relatively limited range of wind speeds, which is why this plot can show the field data without a large scatter in the data points. The solid line shows the relationship (4) found in Fig. 7 for the UCSB tank data.

5. Conclusions

Data from the UCSB wind wave tank have been analyzed in detail. It was found that using nondimensional scaling gives a poor representation of the data with a large scatter in the data points. Multivariate regression showed how to reduce this scatter. In the wave tank environment, H is a function of U^2x and F is a function of $U^{1.25}x$; $H_{sig} \propto (U^2x)^{0.75}$ and $F \propto (U^{1.25}x)^{-0.4}$, respectively. These relationships are inconsistent with the conventional nondimensional equations used to describe wind wave growth. The behavior of wind wave growth in four other wave tanks has also been analyzed, and it was found to be very similar to that observed in the UCSB tank.

The wind speed dependence in a wave tank may be approximated as follows: for a given fetch in the tank, the frequency is inversely proportional to the square root of the wind speed, and the wavelength is proportional to the wind speed. This is true except at very low wind speeds and/or with very short fetches for which the effect of surface tension alters the dispersion relationship. Similarly, the wave height is proportional to $U^{1.5}$, and the orbital velocity is proportional to the wind speed U.

The UCSB results were also found to be broadly consistent with the JONSWAP relationships $F^* = Cx^{*-0.33}$ and $H^* = Dx^{*0.5}$, except that in the wave tank environment neither C nor D are constant; rather, they are a function of the fetch and the square of the wind speed, $C \propto (U^2x)^{-0.1}$ and $D \propto (U^2x)^{0.25}$. An alternative relationship for D was also proposed with $D \propto (U^2x)^{0.15}$, which also fit the data and was consistent with Toba's law. Despite differences in the fetch relationships for the tank and the field, the wave height and wave period satisfy Toba's 3/2 power law. The quantities C and D may be related to the momentum retention and energy retention factors, $(1/\tau)(dM/dt) \propto D^2$ and $(1/E)(dE/dt) \propto (C^{-1.5})^2$, respectively, whose derivation is discussed in the appendix. Both the momentum retention and energy retention factors increased with wind speed and fetch in the short fetch environments investigated here. At longer fetch, both factors should eventually decrease to zero because the waves will reach equilibrium with the wind (i.e., the waves will stop growing). The physical interpretation of this is that in the wave tank environment the dissipation rate relative to the wind pumping decreases with fetch, and the rate of change of wave momentum increases with fetch. Comparisons with field data suggest that the fetch relations may gradually make a transition to the conventional JONSWAP-type fetch laws at longer fetch, and therefore the growth of both the momentum retention and energy retention factors should slow down and eventually decrease.

Acknowledgments. T. Lamont-Smith works for QinetiQ (Ltd) in Malvern, United Kingdom. He was funded by a JSPS Invitation fellowship while carrying out this research as a visiting fellow in the Environmen-

tal and Ocean Engineering Department at the University of Tokyo. Both authors previously worked at the Ocean Engineering Laboratory at UCSB and thank the director of the laboratory, Professor M. P. Tulin. Thanks go in particular to V. Riquelme, who helped to collect the wave wire data, as well as to A. Kolaini, J. Fuchs, and many other colleagues at the laboratory.

APPENDIX

Analytical Derivation of the Fetch Laws

The proportionality constant of the power laws can be obtained following the analyses by Toba (1972) and Tokuda and Toba (1982), which consider the balance of the energy change dE, momentum change dM, and phase speed c_p; thus,

$$dE = c_p dM + M dc_p. \tag{A1}$$

The exact nature of the physics that results in the loss or increase of the energy and momentum will not be considered here. To obtain an evolution equation for the energy and for the phase velocity independently, a constraint on Eq. (A1) needs to be imposed, as follows:

$$\frac{d(\ln H^*)}{d(\ln T^*)} = \frac{s}{2}, \tag{A2}$$

where $H^* = gH/U^2$ and $T^* = gT/U$, as before; and s is the local equilibrium constant, where $s = 3$ is equivalent to Toba's 3/2 law. Condition (A2) imposes a strong constraint that the waves be in local equilibrium. Under steady conditions, the rate of change of energy in fetch can be derived as

$$\frac{dE^*}{dx^*} = \frac{2s^2}{s^2 - 1} G\left(\frac{\rho_a}{\rho_w}\right) C_D \equiv \frac{D^2}{2}, \tag{A3}$$

where C_D is the drag coefficient, ρ_a and ρ_w are the density of air and water, G is the momentum retention factor, as introduced in Toba (1972),

$$G \equiv \frac{1}{\tau}\frac{dM}{dt}, \tag{A4}$$

and τ is the sea surface wind stress. The constant D depends on both the momentum retention factor G and on s, the local equilibrium constant. Assuming that G is weakly dependent on the fetch, or that the waves are in local equilibrium, Eq. (A3) can be integrated to give a fetch law

$$E^* = \frac{D^2}{2} x^*, \tag{A5}$$

which is supported by various observational studies (Table 1).

Following a similar procedure, one can obtain an evolution equation for the phase velocity c_p in dimensional form:

$$\frac{\partial c_p}{\partial x} = \frac{1}{s}\left(\frac{1}{E}\frac{dE}{dt}\right) = A\frac{\dot{e}_w}{E}, \tag{A6}$$

where the energy retention rate A is introduced. Assuming proportionality of wind pumping $\dot{e}_w$ and dissipation D_b, A can then also be expressed as

$$A = \frac{\dot{e}_w - D_b}{\dot{e}_w} = 1 - \frac{D_b}{\dot{e}_w}. \tag{A7}$$

Therefore, an increase in A indicates that the magnitude of dissipation is decreasing relative to the wind pumping. As the waves grow and become equilibrated, the dissipation and wind pumping balance so the wave energy remains constant, that is, $A = 0$. So, for longer fetch, A should eventually decrease with fetch.

Under the assumption that wind pumping and dissipation are proportional, Eq. (A6) can be rewritten utilizing the power law representation of the wave growth rate due to wind pumping, such that

$$\frac{\partial c_p}{\partial x} = \frac{1}{s}\left(\frac{1}{E}\frac{dE}{dt}\right) = \frac{1}{s} A \frac{g}{c_p}\left(\frac{U}{c_p}\right)^{1+r}. \tag{A8}$$

The condition $r = 0$ is equivalent to Snyder's law (Snyder et al. 1981), which is considered to hold for relatively large fetches in the ocean; for $r = 1$, it is equivalent to Plant's wind pumping law (Plant 1982). By nondimensionalizing (A8) and integrating, the fetch law for the nondimensional phase velocity is obtained, once again assuming that A is weakly dependent on fetch; that is,

$$c_p^{*3+r} = \frac{A}{s} x^*. \tag{A9}$$

Here, $c_p^* = c_p/U$, which can be replaced with $F^* = 1/2\pi c_p^*$ to obtain

$$F^* = \frac{1}{2\pi}\left(\frac{A}{s}\right)^{-(1/3+r)} x^{*-(1/3+r)}. \tag{A10}$$

This gives an expression for C in a general form:

$$C = \frac{1}{2\pi}\left(\frac{A}{s}\right)^{-(1/3+r)}. \tag{A11}$$

From Eqs. (A5) and (A10), and noting that (A5) implies $r = 0$, an expression for the constant B for the local equilibrium condition can be derived:

$$B = C^{1.5} D = \sqrt{\left(\frac{1}{2\pi}\right)^3 \left(\frac{s}{A}\right) \frac{4s^2}{s^2 - 1} G\left(\frac{\rho_a}{\rho_w}\right) C_D}. \tag{A12}$$

For the typical case in which Toba's relation is satisfied ($r = 0$ and $s = 3$), the only unknown parameters are the momentum retention factor G and the energy retention factor A. The quantity A in (A11) can be rearranged to

$$A = 3(2\pi C)^{-3}. \tag{A13}$$

This takes a maximum value for $A = 1$ for the no dissipation case; hence, the maximum value of C is around 0.23. From the analysis leading to Eq. (A7), A should start decreasing as the wind wave gets equilibrated. Figure 13 shows how $C^{-1.5}$ varies, and by extension how A varies in the wave tank. This suggests that waves in the tank exhibit a special stage of wave evolution in which the dissipation rate D_b is actually decreasing with fetch relative to the wind pumping for a given wind speed.

For the momentum retention rate, Eq. (A4) can be rewritten as

$$G = \frac{1}{\tau}\frac{dM}{dt} = \frac{\tau_w}{\tau} = 1 - \frac{\tau_t}{\tau}, \tag{A14}$$

where τ_w is the wave-induced stress, τ_t is the turbulent stress, and τ is the total stress. The turbulent stress is responsible for generating the drift current. Figure 13 shows D increasing with wind speed and fetch, and from (A3), $G \propto D^2$. An increase in G therefore indicates an increase in the rate of change of wave momentum or a decrease in the rate of change of the water boundary layer momentum thickness. At larger fetches than in the tank, Janssen (1989) has shown theoretically that τ_w decreases with wave age; that is, as the waves grow with fetch, G decreases.

REFERENCES

Badulin, S. I., A. V. Babanin, V. E. Zakharov, and D. Resio, 2007: Weakly turbulent laws of wind wave growth. *J. Fluid Mech.,* **591,** 339–378.

Battjes, J. A., T. J. Zitman, and L. H. Holthuijsen, 1987: A reanalysis of the spectra observed in JONSWAP. *J. Phys. Oceanogr.,* **17,** 1288–1295.

Burling, R. W., 1959: The spectrum of waves at short fetches. *Dtsch. Hydrogr. Z.,* **12,** 45–64.

Donelan, M. A., J. Hamilton, and W. H. Hui, 1985: Directional spectra of wind-generated waves. *Philos. Trans. Roy. Soc. London,* **315A,** 509–562.

——, M. Skafel, H. Graber, P. Liu, D. Schwab, and S. Venkatesh, 1992: On the growth rate of wind-generated waves. *Atmos.–Ocean,* **30,** 457–478.

Fontaine, E., 2001: On the evolution of high-energy wind-induced ocean waves. *Proc. 20th Int. Conf. on Offshore Mechanics and Arctic Engineering (OMAE 2001),* Rio de Janeiro, Brazil, OMAE, OMAE2001/S&R-2172.

Fuchs, J., and M. P. Tulin, 2000: Experimental scatterer characterisation: The importance and nature of compact scatterers in LGA imaging of the ocean, emphasising micro-breakers. *NATO Research and Technology Sensors and Electronics Technology (RTO SET) Symp.,* RTO MP-60, Laurel, MD, 9-1–9-14.

Hasselmann, K., and Coauthors, 1973: Measurements of wind-wave growth and swell decay during the Joint North Sea Wave Project (JONSWAP). *Dtsch. Hydrogr. Z.,* **A8,** 3–96.

Hwang, P. A., S. Atakturk, M. A. Sletten, and D. B. Trizna, 1996: A study of the wavenumber spectra of short water waves in the ocean. *J. Phys. Oceanogr.,* **26,** 1266–1285.

Janssen, P. A. E. M., 1989: Wave-induced stress and the drag of airflow over sea waves. *J. Phys. Oceanogr.,* **19,** 745–754.

Jones, I. S. F., and Y. Toba, Eds., 2001: *Wind Stress over the Ocean.* Cambridge University Press, 307 pp.

Kahma, K. K., 1981: A study of the growth of the wave spectrum with fetch. *J. Phys. Oceanogr.,* **11,** 1503–1515.

——, and C. Calkoen, 1992: Reconciling discrepancies in the observed growth of wind-generated waves. *J. Phys. Oceanogr.,* **22,** 1389–1405.

Komen, G. J., L. Cavaleri, M. Donelan, K. Hasselmann, S. Hasselmann, and P. A. E. M. Jannsen, 1994: *Dynamics and Modelling of Ocean Waves.* Cambridge University Press, 554 pp.

Lamont-Smith, T., J. Fuchs, and M. P. Tulin, 2003: Radar investigation of the structure of wind waves. *J. Oceanogr.,* **59,** 49–63.

Masuda, A., and T. Kusaba, 1987: On the local equilibrium of winds and wind waves in relation to surface drag. *J. Oceanogr.,* **43,** 28–36.

Mitsuyasu, H., F. Tasai, T. Suhara, S. Mizuno, M. Ohkusu, T. Honda, and K. Rikiishi, 1980: Observations of the power spectrum of ocean waves using a cloverleaf buoy. *J. Phys. Oceanogr.,* **10,** 286–296.

Phillips, O. M., 1977: *The Dynamics of the Upper Ocean.* Cambridge University Press, 344 pp.

Plant, W. J., 1982: A relation between wind stress and wave shape. *J. Geophys. Res.,* **87,** 1961–1967.

Rozenberg, A. D., M. J. Ritter, W. K. Melville, C. G. Gottschall, and A. V. Smirnov, 1999: Free and bound capillary waves as microwave scatterers: Laboratory studies. *IEEE Trans. Geosci. Remote Sens.,* **37,** 1052–1065.

Snyder, R. L., F. W. Dobson, J. A. Elliott, and R. B. Long, 1972: Array measurements of atmospheric pressure fluctuations above surface gravity waves. *J. Fluid Mech.,* **102,** 1–59.

Toba, Y., 1972: Local balance in the air–sea boundary processes. I: On the growth processes of wind waves. *J. Oceanogr.,* **28,** 109–121.

Tokuda, M., and Y. Toba, 1982: Statistical characteristics of individual waves in laboratory wind waves. II. Self-consistent similarity regime. *J. Oceanogr.,* **38,** 8–14.

Tulin, M. P., 1994: Breaking of ocean waves and downshifting. *Waves and Nonlinear Processes,* J. Grue, B. Gjevik, and J. E. Weber, Eds., Kluwer Academic, 177–190.

Walsh, E. J., D. W. Hancock III, D. E. Hines, R. N. Swift, and J. F. Scott, 1989: An observation of the directional wave spectrum evolution from shoreline to fully developed. *J. Phys. Oceanogr.,* **19,** 670–690.

Waseda, T., Y. Toba, and M. P. Tulin, 2001: Adjustment of wind waves to sudden changes of wind speed. *J. Oceanogr.,* **57,** 519–533.

Wilson, B. W., 1965: Numerical prediction of ocean waves in the North Atlantic for December 1959. *Dtsch. Hydrogr. Z.,* **18,** 114–131.